PCCP

RSC Publishing

PAPER

View Article Online
View Journal | View Issue

Cite this: *Phys. Chem. Chem. Phys.*, 2013, **15**, 7123

Long-range Li^+ dynamics in the lithium argyrodite Li_7PSe_6 as probed by rotating-frame spin–lattice relaxation NMR†

V. Epp,*[a] Ö. Gün,[b] H.-J. Deiseroth[b] and M. Wilkening*[a]

Received 5th December 2012,
Accepted 15th March 2013

DOI: 10.1039/c3cp44379e

www.rsc.org/pccp

Lithium-rich argyrodites belong to a relatively new group of fast ion conducting solids. They might serve as powerful electrolytes in all-solid-state lithium-ion batteries being, from a medium-term point of view, the key technology when safe energy storage systems have to be developed. Spin–lattice relaxation (SLR) nuclear magnetic resonance (NMR) measurements carried out in the rotating frame of reference turned out to be the method of choice to study Li dynamics in argyrodites. When plotted as a function of the inverse temperature, the SLR rates $\log_{10}(R_{1\rho})$ reveal an asymmetric diffusion-induced rate peak. The rate peak contains information on the Li jump rate, the activation energy of the hopping process as well as correlation effects. In particular, considering the high-temperature flank of the SLR NMR rate peak recorded in the rotating frame of reference, an activation energy of approximately 0.49 eV is found. This value represents long-range lithium jump diffusion in crystalline Li_7PSe_6. As an example, at 325 K the Li jump rate determined from SLR NMR is in the order of 1.4×10^5 s^{-1}. The pronounced asymmetry of the rate peak $R_{1\rho}(1/T)$ points to correlated Li motion. It is comparable to that which is typically found for structurally disordered materials showing a broad range of correlation times.

I. Introduction

The development of powerful lithium-ion batteries, which are expected to be the intermediate-term devices to store electrical energy, requires the availability and provision of lithium-ion conductors with a very high Li^+ mobility.[1–7] In particular, compared to *liquid* electrolytes, the use of *solid* ion conductors meets the challenges to design more powerful and highly safe lithium-ion batteries.[7,8] These are expected to show a long lifetime which is, in particular, necessary for large-scale, decentralised stationary energy storage. Thus, research on materials for lithium-ion batteries is in line with the imperative goal to reduce our dependence on fossil fuels if we are to store electrical energy from renewable sources and, hence, to combat climate change. Finding suitable solid electrolytes will certainly provide a leap forward towards the development of safe all-solid-state lithium-ion batteries being useful for diverse applications of energy storage systems such as portable electronic devices or even (hybrid) electric vehicles.

During the last few years many Li containing solid electrolytes have been screened and also modified for such purposes. However, the number of suitable candidates turns out to be rather rare, see, *e.g.*, ref. 8–14. Essentially, besides chemical inertness, which oxide materials usually show, they have to fulfill the necessary requirement to exhibit an ionic conductivity exceeding, in the ideal case, 10^{-3} S cm^{-1} at room temperature.

Quite recently, a new class of Li-rich materials has been investigated, *viz.* crystalline lithium argyrodites, which exhibit such a sufficiently high Li^+ mobility.[9,15] So far, Li dynamics of the compounds belonging to the class of Li_7PX_6 (X = S, Se) and Li_6PX_5X' (X′ = Cl, Br, I), which are from a structural point of view closely related to the mineral Ag_8GeS_6, have mainly been investigated by impedance spectroscopy.[9,15–19] Apart from first line shape analyses,[9,15] an in-depth Li nuclear magnetic resonance (NMR) spin–lattice relaxation (SLR) study is still missing. It turned out that the highest conductivity was found for the halides rather than for the pure sulfides or selenides.[15] Apart from impedance spectroscopy, Li jump rates and thus Li

[a] *Christian Doppler Laboratory for Lithium-ion Batteries, Graz University of Technology, Institute for Chemistry and Technology of Materials, Stremayrgasse 9, 8010 Graz, Austria. E-mail: viktor.epp@tugraz.at, wilkening@tugraz.at*
[b] *University of Siegen, Inorganic Chemistry I, Adolf-Reichwein-Straße 2, 57068 Siegen, Germany*

† Electronic supplementary information (ESI) available. See DOI: 10.1039/c3cp44379e

diffusion coefficients can be studied by time-domain Li NMR spectroscopy.[20–26] Compared to conductivity measurements, diffusion-induced Li NMR SLR rates solely reflect Li^+ diffusivity rather than e^- dynamics which might also contribute to the total conductivity probed. In the latter case, contributions arising from other charge carriers have to be carefully eliminated which in some cases might be fraught with great experimental difficulties. By using NMR spectroscopy instead, no special post-preparation of the material to be investigated is necessary and a powdered sample is sufficient to study Li dynamics in detail. Usually the powder is sealed in a small glass ampoule in an inert gas atmosphere to protect it from moisture. Therefore, NMR spectroscopy offers a rather direct and non-destructive access to Li self-diffusion parameters which can easily be converted into (solid-state) Li diffusion coefficients.[27–29]

In the present case, the low-temperature modification of Li_7PSe_6, whose structure has been well characterized by both X-ray powder diffraction and high-resolution NMR recently,[15] was chosen to study dynamic properties by temperature-variable ^{7}Li NMR spectroscopy. The material served as a first model substance to enlighten Li ion transport properties of lithium-rich argyrodites by NMR SLR methods. Here, NMR SLR rate measurements performed in the so-called *rotating* frame of reference turned out to be the best choice to study Li self-diffusion processes. The method takes advantage of an oscillating magnetic field B_1 (rather than the ordinary external magnetic field B_0), which is used to perturb the ^{7}Li spin system in the frame of an SLR NMR experiment.[30,31] The associated radio (or locking) frequency ω_1 is related to B_1 *via* $\gamma B_1 = \omega_1$ where γ is the magnetogyric ratio of the nucleus under investigation. Since ω_1 is in the order of some tens of kHz and ω_0 is in the upper MHz range, NMR SLR measurements performed in the rotating frame of reference are sensitive to Li jump rates with values in the order of 10^4 to 10^5 s^{-1}, thus, considerable longer correlation times can be probed than it is possible with SLR NMR measurements performed in the laboratory frame of reference being the more common technique to probe ion dynamics by NMR.[25,28]

In general, monitoring the complete diffusion-induced SLR NMR rate peak, which is obtained when the SLR rate $R_{1\rho}$ is plotted *vs.* the inverse temperature $1/T$, gives access to both the activation energy E_a and the pre-exponential factor τ_0^{-1} determining the underlying Arrhenius relation (see below). Furthermore, it contains information about correlation effects such as structural disorder and Coulomb interactions.[32] Therefore, it might be useful to roughly evaluate to what extent short-range Li motions influence the $R_{1\rho}$ rates measured and, thus, ion transport parameters.

II. Experiment

Synthesis and characterization of polycrystalline Li_7PSe_6 with μm-sized crystallites (as well as the closely related Li_7PS_6) are described in great detail by Kong *et al.*[15] Both Li_7PS_6 and Li_7PSe_6 exhibit two structural modifications with a fully reversible phase transition at 483 K and 437 K, respectively. While the high-temperature modification shows the typical argyrodite-type structure (space group $F\bar{4}3m$), the crystal structure of the low-temperature modification is closely related to that of the low-temperature form of α-Cu_7PSe_6 crystallizing with orthorhombic symmetry.[15]

^{7}Li NMR measurements were conducted on a high performance digital Bruker Avance III spectrometer in connection with a shimmed cryomagnet of a nominal magnetic field of *ca.* 7 T. This corresponds to a Larmor frequency of $\omega_0/2\pi$ = 116 MHz. A commercial high-temperature probe head (Bruker Biospin) was employed allowing π/2 pulse lengths of about 2.9 μs. The measurements were performed at temperatures ranging from 216 K to 416 K, which were monitored using a Eurotherm temperature controller in combination with a type T thermocouple. Measurements at temperatures down to 112 K were carried out using a cryo probe (Bruker) which was operated by evaporating liquid nitrogen. As compared to the standard probe, the π/2 pulse length of the cryo probe was *ca.* 5.2 μs. Prior to the measurements the sample was vacuum dried and fire sealed in a glass NMR tube of 5 mm in diameter and 3 cm in length.

^{7}Li NMR SLR rates $1/T_1 = R_1$ were acquired by means of the saturation recovery pulse sequence $10 \times \pi/2 - t_d - \pi/2$ which is depicted in Fig. 1(A).[20,33] Here, the initial ten π/2 pulses in rapid succession are used to destroy any longitudinal magnetization M_z before its recovery is recorded as a function of the delay times t_d. ^{7}Li NMR SLR rates $1/T_{1\rho} = R_{1\rho}$ were recorded in the rotating frame of reference (SLRρ). To this end the spin-locking technique[30–36] was employed (see Fig. 1(B)) where the relaxation of the equilibrium magnetization is probed at rather low magnetic field strengths B_1. The corresponding locking frequency

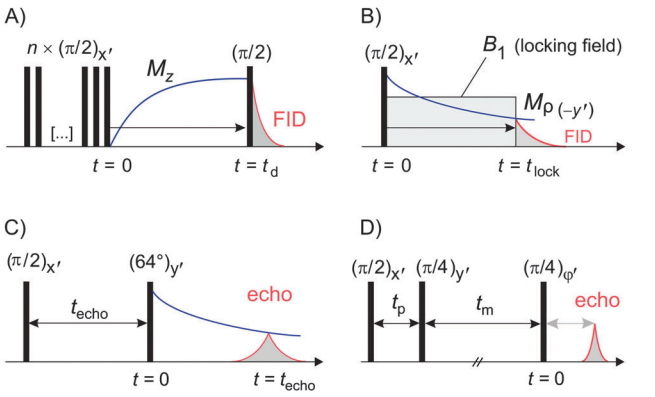

Fig. 1 (A) The saturation recovery pulse sequence used to probe the SLR NMR rates R_1: a comb of closely spaced rf-pulses $(\pi/2)_{x'}$ ($n \approx 10$) destroys the (initial) longitudinal magnetization ($M_z = M_{eq}$) so that $M_z = 0$ at $t = 0$. The subsequent recovery of $M_z(t)$ is probed with a single π/2-pulse which is sent after a variable relaxation delay $t = t_d$. (B) The pulse sequence of the spin-lock technique to record the rotating-frame NMR rates $R_{1\rho}$: immediately after the π/2-pulse the magnetization M pointing along the $(-y')$ is locked by the field B_1. The decay of $M_{\rho(-y')}$ is then probed by plotting the height (or area) of the free induction decay (FID) as a function of the locking pulse length t_{lock}. See also ref. 37. In a simplified manner (C) and (D) depict the pulse sequences to record SSR NMR rates and stimulated echo decay curves. See the text for further explanation.

was chosen to be $\omega_1/2\pi \approx 45$ kHz with the duration of the locking pulse t_{lock} varying between 10 μs and 100 ms. The recycle delay for the SLRρ experiments was set to at least $5 \times 1/R_1$. Both R_1 and $R_{1\rho}$ were obtained by parameterizing the magnetic transients $M_z(t_d)$ and $M_\rho(t_{lock})$, respectively, by stretched exponentials. In the case of $R_{1\rho}$ the exponent γ in $M_\rho(t_{lock}) \propto \exp(-(t_{lock}/T_{1\rho})^\gamma)$ ranges from 0.4 to 0.9 (210 K $\leq T \leq$ 430 K). For the sake of completeness, temperature-variable ^{7}Li NMR spin–spin relaxation (SSR) rates $1/T_2 = R_2$ were monitored, which were recorded using a solid-echo pulse sequence[33] optimized for spin-3/2 nuclei (see Fig. 1(C)). t_{echo} denotes the variable interpulse delay. The corresponding NMR spectra were either obtained after irradiation with a single π/2 pulse or using the solid-echo pulse sequence. In the latter case, echoes were recorded at fixed t_{echo} of 20 μs; spectra were obtained by Fourier transformation beginning from the echo top.

In addition to the SLR and SSR NMR measurements, first ^{7}Li NMR stimulated echoes have been recorded by utilizing the Jeener–Broekaert[38] pulse sequence which is in simplified terms shown in Fig. 1(D).[21,39–41] Usually, such stimulated echo measurements are sensitive to slow Li dynamics.[21,42–48] The technique gives access to single-spin two-time correlation functions[21,22,39] and takes advantage of the different electrical environments the Li spins sense during hopping from site to site. Here, so-called ^{7}Li sin–sin hopping correlation functions,[21,39] *i.e.*, spin-alignment echo (SAE) decay curves,[24,25,43] were monitored at a fixed preparation time t_p of 12 μs and a variable mixing time t_m ranging from 10 μs to 100 s. Appropriate phase cycling is necessary to eliminate unwanted coherences.[39]

III. Results and discussion

Temperature-variable ^{7}Li NMR spectra of crystalline Li_7PSe_6 yield first insights into the Li dynamics of the argyrodite. In Fig. 2 various NMR spectra are shown which were recorded at temperatures ranging from 216 to 417 K. They were acquired using a single pulse sequence, thus, quadrupole intensities (see below) are largely suppressed. Typically, at low temperatures, *i.e.* in the so-called rigid-lattice regime, a dipolar broadened NMR (central) line is observed which can be approximated with a Gaussian. Due to the increasing motion of the Li spins at elevated temperatures dipole–dipole interactions are continuously averaged. Hence, the central NMR line width obeys a motional narrowing (MN) from which the Li jump rate can be roughly estimated. In the present case, even at temperatures as low as 200 K MN has already set in. This can be clearly seen when Fig. 3 is considered where the NMR line width (full width at half maximum), directly read out from the NMR spectra recorded, is plotted *vs. T*. The dashed line is simply drawn to guide the eye; the rigid-lattice regime is reached at temperatures lower than 150 K.

Whereas at the highest temperatures ($T > 350$ K, that is, the regime of extreme narrowing) the NMR central line, corresponding to the spin-quantum transition $I = \pm 1/2 \rightleftarrows I = \mp 1/2$, can be well approximated with a Lorentzian, the NMR line in the intermediate temperature range can be represented by the sum of a Lorentzian line and a Gaussian line. However, a strongly heterogeneous narrowing of the NMR central line, which in many cases is reflected by a pronounced difference in line width of the two components,[50,51] seems to be absent in the present case. Thus, the lack of clearly recognizable two-phase spectra hampers a quantitative analysis according to that, *e.g.*, presented in ref. 52. Nevertheless, the shape of the central transitions shown in Fig. 2(a) points to a distribution of Li jump rates and, therefore, also to a distribution of Li migration pathways in the Li-argyrodite studied.

Since the MN curve shown in Fig. 3 is obtained by plotting the overall line widths of the spectra recorded, it is only of limited use for the extraction of dynamic jump parameters. Significant MN is expected when the jump rate τ^{-1} reaches the order of the rigid lattice line width. For example, one might take use of the inflexion point of the curve ($T_{infl} \approx 235$ K) to estimate τ^{-1}. Using $\nu_{rl} \approx 6.8$ kHz for the NMR line width measured in the rigid lattice regime, the corresponding Li jump rate τ^{-1} is approximately given by ${\tau_{MN}}^{-1} \approx 2\pi \times \nu_{rl} \approx 4 \times 10^4\ s^{-1}$. Moreover, from the so-called onset temperature ($T_{onset} \approx 180$ K) an activation energy $E_{a,MN}$ can be roughly estimated according to the expression of Waugh and Fedin,[53] $E_{a,MN}/meV = 1.62 \times T_{onset}/K$. In the present case this yields $E_{a,MN} \approx 0.3$ eV. However, considering the analysis of Faske *et al.*,[51] in the case of a distribution of lithium jump rates, this approach is at risk to underestimate the activation energy obtained and to overestimate the jump rate deduced from MN, respectively. In particular, this is the case when motion-induced line narrowing spans a broad temperature range, here this is more than 100 K, and T_{onset} is mainly governed by the fraction of fast ions which are presumably subject to, *e.g.*, short-range (or spatially localized) jump processes.[52]

In the present case, a more precise access to Li jump rates is given by SLR NMR. Before discussing the corresponding results, it is useful to have a closer look on the features of the NMR spectra recorded in the rigid-lattice regime and in the limit of extreme narrowing, *i.e.*, at the highest temperatures where the line width is mainly governed by inhomogeneities of the external magnetic field. Interestingly, in the latter regime a well-defined quadrupole powder pattern shows up. Such electric quadrupole intensities are due to the interaction of the quadrupole moment of the 3/2-spin nucleus, which is a result of the non-spherical charge distribution of the nucleus, being immersed in an electronic environment characterized by a non-vanishing electric field gradient (EFG). The latter is produced by the electric charge distribution in the direct neighbourhood of the nucleus under observation. This additional interaction alters the Zeeman levels and thus the associated (angular) Zeeman frequency ω_0 towards $\omega_0 \pm \omega_Q$.[54] The corresponding quadrupole frequency is given by

$$\omega_Q = \pm\delta\pi/2(3\cos^2\Theta - 1 - \eta_Q \sin^2\Theta \cos(2\Phi)) \qquad (1)$$

with the quadrupole coupling constant $\delta = e^2qQ/h$. Here, e and eq are the proton charge and the principle component of the

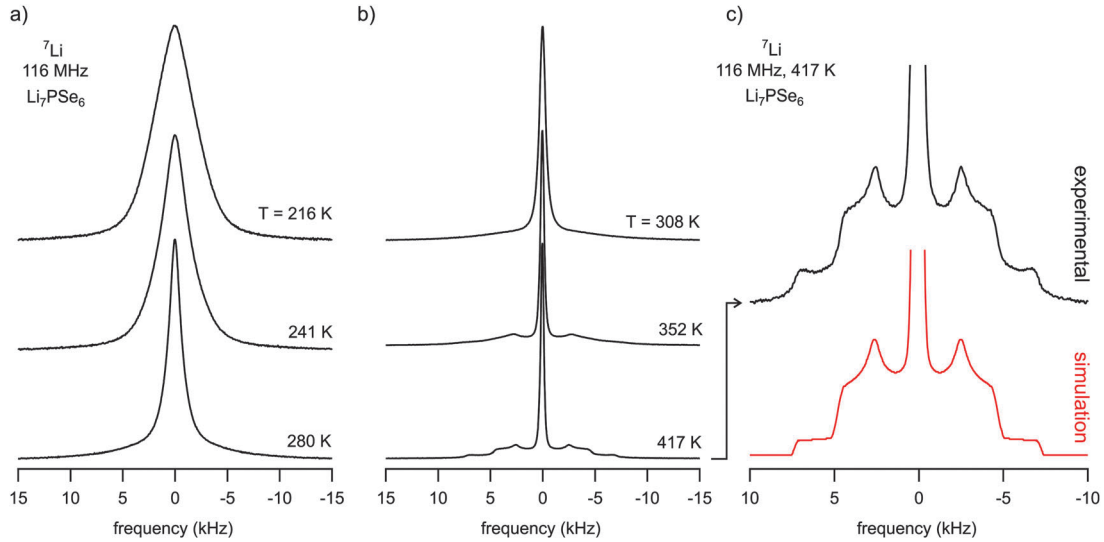

Fig. 2 (a) and (b) ^{7}Li NMR spectra of ternary Li_7PSe_6 recorded at the temperatures indicated. The line width steadily decreases reflecting a pronounced motional narrowing which indicates rapid Li exchange on the NMR time scale defined by the rigid lattice line width of Li_7PSe_6. Pronounced and well-defined quadrupole powder patterns emerge at temperatures chosen to be higher than 300 K. It is fully developed at 417 K. (c) Magnification of the quadrupole powder pattern of the ^{7}Li NMR recorded at 417 K. The spectrum shown at the bottom displays a simulation of the measured one with the help of WinSolids software[49] using a single set of fitting parameters describing the NMR line shape. See the text for further details.

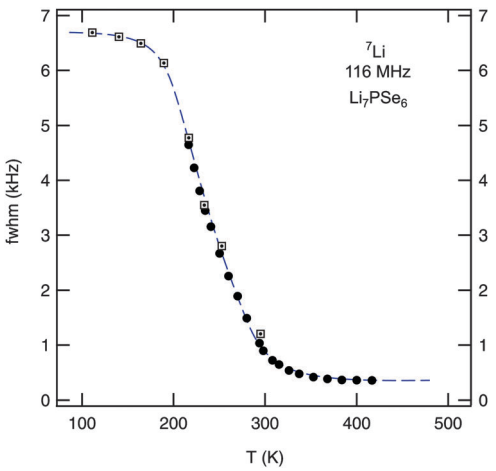

Fig. 3 Motional narrowing of the ^{7}Li NMR linewidth of polycrystalline Li_7PSe_6. While filled symbols (●) represent data points recorded using a standard probe, boxes display the line widths (fwhm) of NMR spectra recorded using a cryo probe. The rigid lattice value, $\nu_{rl} \approx 6.8$ kHz, is reached at temperatures below 150 K. The onset of MN is expected when the Li jump rate reaches values in the order of 10^3 s^{-1}. See the text for further explanation.

electric field gradient tensor, respectively. Q is the electric quadrupole moment of the ^{7}Li nucleus and h denotes Planck's constant. The angles Θ and Φ specify the orientation of the external field B_0 in the principle axis system of the EFG tensor at the site of the ^{7}Li spin. The parameter η_Q reflects any asymmetries of the EFG tensor. Here, the ^{7}Li NMR line recorded at 417 K can be well represented by a quadrupole powder pattern with $\delta = 14.6$ kHz and $\eta_Q = 0.6$. Certainly, the values should be regarded as mean values characterizing the EFG tensor the Li spins are exposed to due to rapid hopping at elevated temperatures. In the low-temperature modification of Li_7PSe_6 the Li ions occupy electrically (and magnetically) inequivalent crystallographic sites. In general, the absence of a complete averaging of electric quadrupole interactions at high T has been found for many Li ion conductors and might be regarded as a universal feature.[47,55,56] It is referred to as anisotropic (or inhomogeneous) diffusion which is certainly traced back to the complex crystal structure of the lithium-containing argyrodite under investigation, *cf.* also Fig. 7 in ref. 16.

In the absence of lithium motions on the kHz scale, quadrupole intensities in the rigid-lattice regime can be made visible by recording NMR solid echoes. Owing to receiver dead-time effects, fast decaying components of an FID are difficult to detect. In Fig. 4 an NMR spectrum recorded in the rigid-lattice regime is shown which has been acquired at 190 K with the help of a two-pulse solid-echo sequence. Besides the Gaussian shaped central line, whose area fraction is about 36% of the total area, a broad quadrupole foot (64%) becomes apparent. The width (fwhm) of the latter component is about 54 kHz and points to a mean rigid-lattice quadrupole coupling constant in the order of 100 kHz. This value is comparable with those of other Li ion conductors studied. With increasing temperature, the rigid-lattice quadrupole interactions are partly averaged due to Li motions with rates as high as 10^5 s^{-1}. Finally, the well-defined powder pattern, as characterized above, shows up at higher T.

As mentioned above, straightforward insights into the Li dynamics in the ternary argyrodite are provided by analyzing diffusion-induced ^{7}Li NMR SLR rates.[20,21,23–28,37,57,58] In Fig. 5 the $R_{1\rho}$ rates measured in both the laboratory and rotating frames of reference are shown in an Arrhenius plot. The R_1 rates reveal a

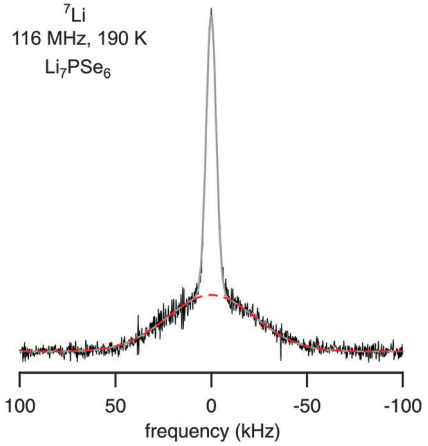

Fig. 4 ^{7}Li solid-echo (first-order quadrupolar) NMR spectrum recorded using a two-pulse sequence at 116 MHz and 190 K. The area fractions of the dipolar broadened central and quadrupole contribution are in agreement with the theoretical ratio of 4 : 6. Upon increasing temperature, the central line and the broad quadrupole signal narrow due to rapid Li exchange.

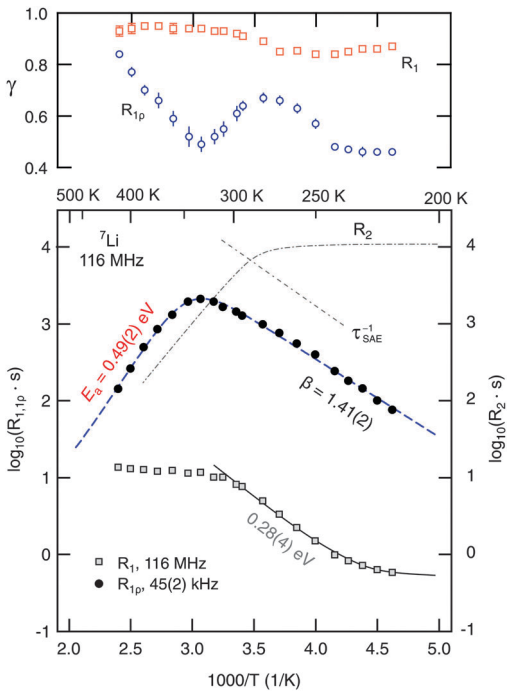

Fig. 5 Arrhenius plot of the ^{7}Li NMR SLR rates measured at a Larmor frequency $\omega_0/2\pi$ of 116 MHz (R_1) and a locking frequency $\omega_1/2\pi$ of 45(2) kHz ($R_{1\rho}$). The dashed line represents a modified BPP fit taking into account a sub-quadratic frequency dependence of the $R_{1\rho}$ rates ($R_{1\rho} \propto \omega_1^{-\beta}$, $\beta < 2$) in the limit $\omega_1\tau \gg 1$. The upper figure shows the temperature dependence of γ used to parameterize the corresponding magnetization transients. For comparison, the temperature behaviour of the R_2 SSR NMR rates and the decay rates deduced from stimulated echo NMR (see the inset of Fig. 7) are also shown. See the text for further explanation.

diffusion-induced low-temperature flank pointing to a relatively small activation energy of only 0.28(1) eV. The so-called low-T regime of NMR SLR is sensitive to short-range rather than to long-range lithium diffusion.[20] Interestingly, the SLR rates probed in the laboratory frame of reference do not exhibit a $R_1(1/T)$ rate peak; above 300 K the rates are independent of temperature and amount to be about 10 s^{-1}. Note that at $T < 235$ K the rates are increasingly governed by non-diffusive and weakly temperature-dependent background effects which, most likely, can be ascribed to coupling of the Li spins with paramagnetic impurities. However, in the case of NMR SLR measurements in the rotating frame of reference performed at a locking frequency in the order of 45 kHz the $R_{1\rho}$ rates pass through a well-defined maximum showing up at T_{max} = 325 K. This allows the direct determination of the Li jump rate τ^{-1} which can be estimated using the maximum condition $\omega_1\tau \approx 0.5$. Note that this estimation is based on an exponential correlation function $G(t)$ leading to symmetric NMR rate peaks (see below). Here, at T_{max} the rate τ^{-1} is in the order of 1.4 × 10^5 s^{-1}. Compared to the result from NMR motional narrowing it becomes evident that the rate τ_{MN}^{-1} seems to overestimate the jump process because of the reasons discussed above.

A more detailed analysis is achieved by using an appropriate relaxation model[20,59] to evaluate the SLR NMR rates $R_{1\rho}(1/T)$ measured. The dashed line shown in Fig. 5 represents a complete relaxation fit according to

$$R_{1\rho}(\omega_1, T) \propto J^{3D}(\omega_1, T) \propto \tau_c/(1 + (2\omega_1\tau_c)^{\beta}). \qquad (2)$$

Note that the correlation rate τ_c^{-1} is in the order of the jump rate τ^{-1}. In general, J^{3D} denotes the spectral density function characterizing electric and magnetic field fluctuations due to three-dimensional ion hopping. Here, the expression of the spectral density function, to which $R_{1\rho}(\omega_1, T)$ is proportional, is based on the relaxation model of Bloembergen, Purcell and Pound (BPP) introduced for 3D, isotropic diffusion.[60] Originally, the exponent β is given by $\beta = 2$, which originates from the assumption of an underlying single exponential motional correlation function $G(t)$. J^{3D} is obtained from $G(t)$ by Fourier transformation. In the case of $\beta = 2$ this results in a symmetric (Lorentzian shaped) spectral density function J^{3D}.[20] Values smaller than two (for β the range $1 < \beta \leq 2$ is valid) as introduced by Küchler *et al.*[61] lead to asymmetric NMR SLR rate peaks whereby the slope of the low-temperature flank, that is the regime where $\omega_1\tau \gg 1$ holds, is smaller than that of the corresponding high-temperature side characterized by the limit $\omega_1\tau \ll 1$. In particular, asymmetric NMR SLR rate peaks have been observed for structurally disordered ion conductors. Theoretical investigations show that Coulomb interactions of the moving ions and/or structural disorder seem to be responsible for the asymmetries observed in NMR relaxometry.[62–64] A pronounced heterogeneous dynamics, being closely related to structural disorder which can be represented by an irregular formed potential landscape, is expected to include both long-range dynamics as well as localized hopping processes.

In the present case, the $R_{1\rho}(\omega_1,T)$ data can be best represented by a fit with β = 1.41(2). This result certainly points to a non-exponential motional correlation function. It might directly

reflect a heterogeneous potential landscape the Li ions are exposed to. In Li_7PSe_6 the Li ions occupy multiple, distinctly connected sites as revealed by high-resolution ^{6}Li NMR spectroscopy.[15] A relatively low β value, as found here, is comparable to that recently reported for Li ion hopping in $Li_7La_3Zr_2O_{12}$ (LLZ); LLZ also exhibits a highly complex crystallographic structure where the Li ions are distributed among various inequivalent positions. Let us mention that $\beta < 2$ minimally influences the maximum condition used above to estimate the jump rate at the temperature where the rate peak shows up. Taking into account $\beta = 1.41(2)$, the exact maximum condition is given by

$$\omega_1\tau = 0.5(\beta - 1)^{-1/\beta} \approx 0.94 \quad (3)$$

provided J^{3D} is restricted to a single term as done in eqn (2), which turns out be a very good approximation.

With E_a (0.49(2) eV) and ${\tau_{c,0}}^{-1} \approx {\tau_0}^{-1}$ ($1.6(9) \times 10^{13}$ s^{-1}) available from the relaxation fit,[65] the jump rate following the Arrhenius relation $\tau^{-1} = {\tau_0}^{-1}\exp(-E_a/(k_BT))$ can be determined. Here, k_B denotes Boltzmann's constant. At ambient temperature, this yields $\tau^{-1} \approx 9.5 \times 10^4$ s^{-1}. Using the Einstein–Smoluchowski equation, which relates τ^{-1} with the self-diffusion coefficient D_{sd} *via*

$$D_{sd} = a^2/(6\tau) \quad (4)$$

it turned out that D_{sd} is $1.3(8) \times 10^{-15}$ m^2 s^{-1} at $T = 300$ K. Here, the jump distance a was estimated to be $a \approx 2.9$ Å which is based on the structural data given in ref. 15. With D_{sd} the corresponding ion conductivity can also be determined *via* the Nernst–Einstein equation. According to this relation the so-called solid-state diffusion coefficient D_{NE} is obtained which is given by

$$D_{NE} = \frac{\sigma_{dc}k_BT}{Nq^2} \quad (5)$$

N denotes the charge carrier density and q represents the charge of the Li ions. σ_{dc} is the ionic dc conductivity. Note that D_{NE} is directly linked with D_{sd} according to $D_{NE} = f/H_R\, D_{sd}$. Here, H_R is the Haven ratio and f denotes the so-called correlation factor. In the present case we assumed $f/H_R \approx 1$ to estimate the ionic conductivity σ_{dc}. Once again, N has been estimated based on the crystallographic data recently obtained for Li_7PSe_6.[15] With D_{sd} given above, the ionic conductivity turns out to be in the order of 2×10^{-6} S cm^{-1} at 300 K. This is in reasonably good agreement with preliminary conductivity measurements on similar samples.[16] It should be noted that even higher ion conductivities have been probed for some halide-containing Li-argyrodites.[9,16,17]

Identifying $E_a = 0.49(2)$ eV (see above) with the activation energy reflecting long-range Li diffusion in Li_7PSe_6, the slope of the low-T flank of the rate peak of Fig. 5 might be related to Li jump processes taking place on a much shorter length scale. This is expressed by $\omega_1\tau \gg 1$ being valid in this temperature range. In the present case, the low-T flank is characterized by $E_{a,low} = 0.21(1)$ eV, thus, fulfilling the relation $E_{a,low} = (\beta - 1)E_a$. It directly links the frequency dependence of $R_{1\rho} \propto {\omega_1}^{-\beta}$ to the asymmetry of the diffusion-induced relaxation rate peak $R_{1\rho}(1/T)$. Indeed, the crystallographic structure of Li-containing argyrodites contains structural motifs, *viz.* Li ions residing in close-by tetrahedral voids, which might help explain the differences between localized, *i.e.*, short-range Li dynamics on the one hand and long-range Li diffusion on the other hand.[15] This is also supported by recent theoretical investigations on halide-containing Li-argyrodites.[16,17]

For comparison with the SLR NMR rates, the γ exponents describing the deviation of the magnetization transients $M_\rho(t_{lock})$, see Fig. 6, from single-exponential time behaviour are also included in Fig. 5. Whereas a straightforward interpretation of γ is generally not available, one might read out two features showing up in the present case. At very low temperatures the exponent is approximately 0.5 which might point to (diffusion-induced) spin–lattice relaxation due to coupling of the ^{7}Li spins primarily to paramagnetic impurities. At even lower temperatures homonuclear spin-diffusion might play an additional role. With increasing diffusivity, γ initially increases before a minimum value is attained at T_{max} where the corresponding maximum peak $R_{1\rho}(1/T)$ shows up. Interestingly, when T is further increased and Li diffusion becomes rapid the exponent γ steadily increases towards $\gamma = 1$, *i.e.*, single-exponential time behaviour. Note that at very high temperatures the various electrical interactions the Li spins are exposed to are greatly averaged resulting in a quadrupole powder pattern which can be simulated with a single set of (mean) parameters. Thus, when considering the underlying motional correlation function, being at least partly reflected by the exponent γ, it might also change as a function of temperature and seems to tend to become a single exponential in the limit $\omega_1\tau \ll 1$. Such an observation is in agreement with the predictions of Ngai and co-workers,[66] who have analyzed the shape of motional correlation functions from both NMR and impedance spectroscopy measurements.

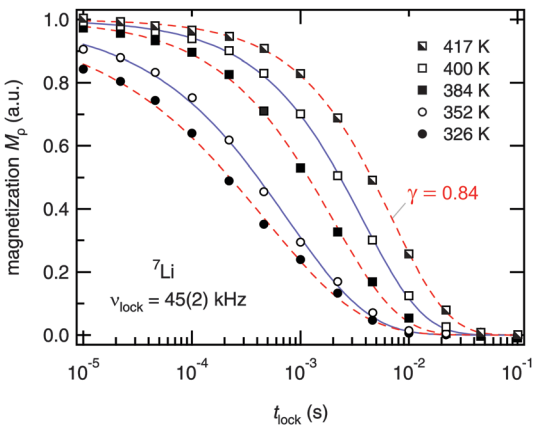

Fig. 6 ^{7}Li NMR magnetization transients $M_\rho(t_{lock})$ of Li_7PSe_6 recorded at the temperatures indicated and at $\omega_0/2\pi = 116$ MHz and $\omega_1/2\pi = \nu_1 = 45(2)$ kHz. Dashed and solid lines represent fits according to $M_\rho(t_{lock}) \propto \exp(-(t_{lock}/T_1)^\gamma)$. At high temperatures, *i.e.* in the limit $\omega_1\tau \gg 1$, the stretching exponent γ increases towards single exponential time behaviour. The decay curves recorded above 360 K represent magnetization transients of the high-temperature flank of the $R_{1\rho}(1/T)$ peak shown in Fig. 5.

For the sake of completeness, R_2 SSR NMR rates were recorded at temperatures down to 190 K. In the rigid-lattice regime, T_2 is approximately 70 μs. This is in good agreement with the second moment, *i.e.*, the line width of the central transition in this temperature range (6.8 kHz), see above. It is worth mentioning that, as expected, the ^{7}Li NMR solid echoes are composed of a fast and slowly decaying contribution which mirror quadrupolar and dipolar contributions. Irrespective of what is analyzed in detail, *i.e.*, (i) the complete area under the echo, (ii) the amplitude of the quadrupole part or (iii) the area of the slowly decaying dipolar part, at very low T the corresponding transients follow single-exponential time behaviour (see Fig. S1 and S2, ESI†). However, the situation changes upon increasing T. Then, a fast decaying and temperature independent contribution with $R_{2'} = 30$ μs shows up (see Fig. S2, ESI†). These rates might reflect a very slow dynamic process. Interestingly, the stimulated echoes, which are presented below, also seem to point to a subset of lithium ions with a very low diffusivity.

For comparison, in Fig. 5 the temperature-dependent R_2 rates of the slowly decaying part of the transients are included. The rates start to decrease at $T = 260$ K. At this temperature the associated jump rate is in the order of 10^4 s^{-1}, which is in good agreement with the Arrhenius parameters deduced from the $R_{1\rho}(1/T)$ peak. However, the corresponding activation energy, which can be estimated from the linearly decaying part of the R_2 curve, turns out to be only 0.4 eV (see also Fig. S2, ESI†). Moreover, the maximum $R_{1\rho}$ rate exceeds R_2. Similarly, this has been observed by, *e.g.*, Bertermann *et al.*[56] who recorded R_2 rates using a Hahn echo pulse sequence. In doing so, Hahn echo decay seems to be determined by dipolar rather than by quadrupolar interactions as expected.

The present difference between $R_{1\rho}$ and R_2 also indicates that the two rates probed are not necessarily influenced by exactly the same relaxation mechanism and/or the same subset of (differently coupled) Li spins. Considering the pre-factor obtained from the $R_{1\rho}(1/T)$ fit ($R_{1\rho} = C' \times J^{3D}(2\omega_1)$), which amounts to $C' = 2.95(9) \times 10^9$ s^{-2}, thus, being in the order of the square of the rigid-lattice quadrupole coupling constant (see above), we suppose that, besides dipolar ones, fluctuating quadrupolar interactions also play a large role in influencing $R_{1\rho}$. However, a conclusive answer to what extent dipolar interactions affect the SLR NMR rates probed might only be possible by future ^{6}Li NMR experiments carried out at resonance frequencies comparable to those used for the ^{7}Li NMR measurements.

In addition to NMR SLR measurements in the rotating frame of reference, we have recorded ^{7}Li spin-alignment echo NMR decay curves which are sensitive to slow Li exchange processes between electrically inequivalent Li sites in the argyrodite. Thus, the method takes advantage of the distinct quadrupolar interactions of the jumping Li ions. The decay curves shown in Fig. 7 were obtained by plotting the intensity of the spin-alignment echo (read out at the echo maximum, *i.e.*, at $t = t_p$) as a function of mixing time. The S_2 curves reflect the probability to find an Li nuclear spin, which initially ($t_m = 0$) resides on a specific site, on an electrically equivalent site at a later time ($t = t_m$).

Interestingly, echo damping proceeds in two steps.[22,26,67] Most likely, the first decay step directly reflects Li hopping; the second step, however, might be induced by (quadrupolar) spin–lattice relaxation and/or spin-diffusion effects. The latter are expected to be characterized by a decay rate τ'' being in the order of seconds. The full decay curves were parameterized with a combination of two stretched exponentials according to

$$S_2(t_p, t_m, t = t_p) = \left(A e^{-(t_m/\tau_{SAE})^{\gamma_{SAE}}} + B\right) e^{-(t_m/\tau'')^{\gamma''}} \qquad (6)$$

Below 270 K, the stretching parameter γ_{SAE} is approximately 0.5. It decreases with increasing T reaching $\gamma_{SAE} \approx 0.25$ at ambient temperature. The fits yield the decay rates τ_{SAE}^{-1} shown in the inset of Fig. 7. Obviously, the first decay step points to Li jumps which are thermally activated similar to those being responsible for motion-induced SLR NMR in the limit $\omega_0\tau \gg 1$ (see above). Note that in other cases SAE NMR has been proven to be very successful in characterizing long-range ion transport properties.[25,51,68–70] In the examples studied so far, the corresponding activation energy $E_{a,SAE}$ turned out to be very similar to the value $E_{a,dc}$ deduced from dc-conductivity measurements. However, in the present case, low-temperature echo damping seems to be mainly influenced by a diffusion process with a much lower thermal activation. This behaviour might change when ^{6}Li (spin-1 nucleus) stimulated echoes are recorded instead of ^{7}Li (spin-3/2 nucleus) echoes. This is because the latter are exposed to rather large homonuclear dipole–dipole interactions which might strongly influence the generation of a pure spin-alignment state.

Irrespective of this possible influence on the ^{7}Li NMR S_2 curves, even at temperatures as low as 220 K the two-step decay behaviour remains. For example, the (normalized) correlation

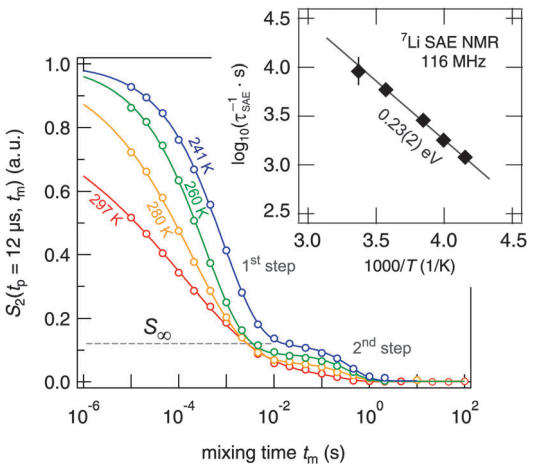

Fig. 7 ^{7}Li NMR (sin–sin) two-time correlation functions recorded using the Jeener–Broekaert[38,39] pulse sequence (116 MHz, $t_p = 12$ μs). While the first decay step of the S_2 decay curve reflects Li hopping between electrically inequivalent Li sites in crystalline Li_7PSe_6, the second one is induced by (quadrupolar) spin–lattice relaxation. Solid lines represent fits with a combination of two stretched exponentials.

function recorded at 241 K is characterized by a so-called plateau value $S_\infty = B/(A + B)$ (see eqn (6)) which is approximately 0.12. In general, $1/S_\infty$ is related to the number of electrically inequivalent Li sites the ion visits during self diffusion.[39] The inverse, $1/S_\infty$, equals the number of available Li sites provided these are equally populated and visited by the spins with the same probability. S_∞ = 0.12 leads, at first glance, to approximately eight different Li sites. In fact, there are at least seven electrically inequivalent Li sites occupied in Li_7PSe_6. It is worth mentioning that, once again, ^{7}Li–^{7}Li dipole–dipole interactions might influence $1/S_\infty$ which usually point to a larger number of sites than actually present in the crystal structure. Such a situation has also been found for SAE NMR measurements on β-eucryptite, $LiAlSiO_4$, single crystals.[71] With increasing temperature T, the value S_∞ decreases which might be attributed to the increasing averaging of electric quadrupolar as well as magnetic dipolar interactions due to sufficiently fast Li hopping.

Alternatively, the emergence of a distinct plateau might also be interpreted in terms of a small and decoupled sub-ensemble of very slow Li ions that show up at large mixing times and low temperature. However, since the corresponding decay rates associated with the second step ($1/\tau''$) do not reveal a significant temperature dependence, the above-given explanation, pointing to the averaging of quadrupole interactions, seems to be more suitable to understand the NMR response. Moreover, at higher temperatures the jump process occurring during the evolution period determined by t_p might also affect the correlation functions probed. This phenomenon is called *motional phase averaging*, see ref. 21 for further details.

In contrast to the diffusion process being responsible for the maximum of $R_{1\rho}(1/T)$, the first decay step of the SAE NMR decay curves reflects Li spins diffusing on a rather long time scale. In this context it is worth mentioning once again that, in general, SAE NMR is insensitive to Li^+ jumps between electrically inequivalent sites. This also holds for sufficiently fast exchange processes for which echo formation is not possible or for hopping processes leading to elimination of fluctuating EFGs. The latter means fast jump processes involving a small number of preferred but electrically inequivalent sites. Such a process would lead to an averaged but mixing-time independent EFG and is expected to contribute to SLR NMR but it would be invisible for SAE NMR. This view might help understand the difference found between τ^{-1} from $R_{1\rho}(1/T)$ and $\tau_{SAE}{}^{-1}$. Such a scenario of fast and slowly diffusing spins,[16] which allow exchange between each other, is also in agreement with a relatively large final state amplitude for the slow process most likely involving the majority of the Li sites available. As mentioned above, exchange between closely adjacent voids in Li_7PSe_6, see ref. 15 and 16, might represent such a preferred (spatially localized and fast) hopping process to which SAE NMR is not sensitive, *cf.* also the illustration of Fig. 7 in ref. 16. The relatively low activation energy deduced from SAE NMR might point to the conclusion that at higher T further hopping processes come into play which are finally detected by $R_{1\rho}(1/T)$ in the high-temperature limit.

For comparison with a recent study on Li_4SnS_4, let us note that Dehnen and co-workers[72] reported on SAE data which reveal low-temperature echo decay damping pointing to an extremely slow Li motional process. This process is reported to be thermally activated by 0.05 eV only. Very recently, by our own group a similar motion process with an activation energy of 0.09 eV was observed for a structurally disordered ion conductor. In contrast to the SAE NMR response probed here, but in analogy to the well-known *nearly constant loss* (NCL) phenomenon in conductivity spectroscopy, in ref. 73 we interpreted this feature as a result from strictly localized (or caged) motions, see also ref. 74.

Finally, instead of a single (Arrhenius-type) diffusion process we found indications for various motional mechanisms present in Li_7PSe_6. This also includes the possibility that diffusion mechanisms change as a function of temperature and dominate others in certain ranges. It also helps understand why it is hardly possible to perform a so-called joint fit, see, *e.g.*, ref. 28, of the temperature-variable and frequency-dependent SLR NMR rates $R_{1\rho}$ and R_1. Here, the rates R_1 might be interpreted as the result of a superposition of different processes leading to 0.28 eV (Fig. 5) in the end. In contrast, long-range Li^+ ion dynamics at higher T seem to be determined by an activation energy of 0.49 eV which can be deduced from the $R_{1\rho}(1/T)$ peak in the relaxation limit $\omega_1\tau_c \ll 1$.

IV. Conclusion and outlook

In summary, local electric structures and Li self-diffusion in a polycrystalline sample of Li_7PSe_6 have been examined by temperature-variable ^{7}Li NMR spectroscopy. Line shape as well as SLR measurements have been used to get insights into translational Li dynamics present. While the first seem to be mainly governed by local exchange processes, with the help of SLR measurements short- as well as long-range diffusion parameters are accessible. In particular, it turned out that SLR measurements performed in the rotating frame of reference are highly suited to characterize Li hopping motions taking place on different length scales in the Li-containing argyrodite. From the diffusion-induced $R_{1\rho}$ SLR rate peak probed, both the activation energy (0.49(2) eV) as well as the pre-exponential factor ($1.6(9) \times 10^{13}$ s^{-1}) of the underlying Arrhenius relation characterizing long-range dynamics (at higher T) could be probed. At ambient temperature, the Li self-diffusion coefficient is approximately $1.3(8) \times 10^{-15}$ m^2 s^{-1}. This points to an Li ion conductivity in the order of 2×10^{-6} S cm^{-1} at 300 K. In contrast, at lower T Li dynamics seem to be characterized by activation energies ranging from 0.21 eV ($R_{1\rho}$) to 0.28 eV (R_1). Most likely, the relevant diffusion processes being valid in this T range also entail short-range dynamics.

The measurements carried out so far build a helpful basis to be used for the comparison with halide containing Li-argyrodites such as Li_6PSe_5Cl revealing even higher Li conductivities.[9,15,17–19,75] Currently, chlorine-containing and bromine-containing argyrodites are investigated in our laboratory. In addition to the first ^{7}Li SAE NMR measurements presented here, the analysis of

^{6}Li NMR hopping correlation functions might be very useful to shed more light on the dynamic processes probed *via* the generation of stimulated echoes.

Acknowledgements

We thank G. Schmidt (Bruker, Karlsruhe (Germany)) for his help with setting up the NMR spectrometer at the TU Graz and greatly appreciate the valuable comments of an unknown referee. Financial support from the Austrian Federal Ministry of Economy, Family and Youth, and the Austrian National Foundation for Research, Technology and Development as well as by the Deutsche Forschungsgemeinschaft (DFG) is highly appreciated (DFG Research Unit 1277).

References

1 M. S. Whittingham, *Chem. Rev.*, 2004, **104**, 4271.
2 J. M. Tarascon and M. Armand, *Nature*, 2001, **414**, 359.
3 M. Armand and J.-M. Tarascon, *Nature*, 2008, **451**, 652.
4 J.-M. Tarascon, *ChemSusChem*, 2008, **1**, 777.
5 M. Winter and J. O. Besenhard, *Electrochim. Acta*, 1999, **45**, 31.
6 A. S. Aricó, P. Bruce, B. Scrosati, J.-M. Tarascon and W. V. Schalkwijc, *Nat. Mater.*, 2005, **4**, 366.
7 J. B. Goodenough and Y. Kim, *Chem. Mater.*, 2010, **22**, 587.
8 P. Knauth, *Solid State Ionics*, 2009, **180**, 911.
9 H.-J. Deiseroth, S.-T. Kong, H. Eckert, J. Vannahme, C. Reiner, T. Zaiss and M. Schlosser, *Angew. Chem., Int. Ed.*, 2008, **47**, 755.
10 Y. Zhao and L. L. Daemen, *J. Am. Chem. Soc.*, 2012, **134**, 15042.
11 A. Hayashi and M. Tatsumisago, *Electron. Mater. Lett.*, 2012, **8**, 199.
12 N. Kamaya, K. Homma, Y. Yamakawa, M. Hirayama, R. Kanno, M. Yonemura, T. Kamiyama, Y. Kato, S. Hama and K. Kawamoto, *et al.*, *Nat. Mater.*, 2011, **10**, 682.
13 H. Buschmann, J. Dölle, S. Berendts, A. Kuhn, P. Bottke, M. Wilkening, P. Heitjans, A. Senyshyn, H. Ehrenberg and A. Lotnyk, *et al.*, *Phys. Chem. Chem. Phys.*, 2011, **13**, 19378.
14 S. Narayanan, V. Epp, M. Wilkening and V. Thangadurai, *RSC Adv.*, 2012, **2**, 2553.
15 S. T. Kong, O. Gün, B. Koch, H. J. Deiseroth, H. Eckert and C. Reiner, *Chem.–Eur. J.*, 2010, **16**, 5138.
16 O. Pecher, S.-T. Kong, T. Goebel, V. Nickel, K. Weichert, C. Reiner, H.-J. Deiseroth, J. Maier, F. Haarmann and D. Zahn, *Chem.–Eur. J.*, 2010, **16**, 8347.
17 R. P. Rao and S. Adams, *Phys. Status Solidi A*, 2011, **208**, 1804.
18 P. R. Rayavarapu, N. Sharma, V. K. Peterson and S. Adams, *J. Solid State Electrochem.*, 2012, **16**, 1807.
19 S. Boulineau, M. Courty, J.-M. Tarascon and V. Viallet, *Solid State Ionics*, 2012, **221**, 1.
20 P. Heitjans, A. Schirmer and S. Indris, in *Diffusion in Condensed Matter*, ed. P. Heitjans and J. Kräger, Springer, 2005, ch. 9, p. 367.
21 R. Böhmer, K. Jeffrey and M. Vogel, *Prog. Nucl. Magn. Reson. Spectrosc.*, 2007, **50**, 87.
22 C. Brinkmann, S. Faske, B. Koch and M. Vogel, *Z. Phys. Chem.*, 2010, **224**, 1535.
23 V. Epp and M. Wilkening, *Phys. Rev. B: Condens. Matter Mater. Phys.*, 2010, **82**, 020301.
24 M. Wilkening, J. Heine, C. Lyness, A. R. Armstrong and P. G. Bruce, *Phys. Rev. B: Condens. Matter Mater. Phys.*, 2009, **80**, 064302.
25 M. Wilkening and P. Heitjans, *ChemPhysChem*, 2012, **13**, 53.
26 M. Wilkening and P. Heitjans, *Phys. Rev. B: Condens. Matter Mater. Phys.*, 2008, **77**, 024311.
27 M. Wilkening, A. Kuhn and P. Heitjans, *Phys. Rev. B: Condens. Matter Mater. Phys.*, 2008, **78**, 054303.
28 A. Kuhn, S. Narayanan, L. Spencer, G. Goward, V. Thangadurai and M. Wilkening, *Phys. Rev. B: Condens. Matter Mater. Phys.*, 2011, **83**, 094302.
29 A. Kuhn, J.-Y. Choi, L. Robben, F. Tietz, M. Wilkening and P. Heitjans, *Z. Phys. Chem.*, 2012, **226**, 525.
30 D. Ailion and C. P. Slichter, *Phys. Rev. Lett.*, 1964, **12**, 168.
31 C. P. Slichter and D. Ailion, *Phys. Rev. Sect. A*, 1964, **135**, A1099.
32 E. Fukushima and S. B. W. Roeder, *Experimental Pulse NMR: A Nuts and Bolts Approach*, Addison-Wesley Pub. Co., Advanced Book Program, Reading, Mass., 1981.
33 D. C. Ailion and C. P. Slichter, *Phys. Rev. Sect. A*, 1965, **137**, A235.
34 D. C. Look and I. J. Lowe, *J. Chem. Phys.*, 1966, **44**, 2995.
35 T. J. Rowland and F. Y. Fradin, *Phys. Rev.*, 1969, **182**, 760.
36 D. Wolf, *Phys. Rev. B: Solid State*, 1974, **10**, 2724.
37 A. Kuhn, M. Kunze, P. Sreeraj, H. D. Wiemhöfer, V. Thangadurai, M. Wilkening and P. Heitjans, *Solid State Nucl. Magn. Reson.*, 2012, **42**, 2.
38 J. Jeener and P. Broekaert, *Phys. Rev.*, 1967, **157**, 232.
39 R. Böhmer, *J. Magn. Reson.*, 2000, **147**, 78.
40 X.-P. Tang, R. Busch, W. Johnson and Y. Wu, *Phys. Rev. Lett.*, 1998, **81**, 5358.
41 X.-P. Tang, U. Geyer, R. Busch, W. Johnson and Y. Wu, *Nature*, 1999, **402**, 160.
42 R. Böhmer, T. Jörg, F. Qi and A. Titze, *Chem. Phys. Lett.*, 2000, **316**, 419.
43 F. Qi, T. Jörg and R. Böhmer, *Solid State Nucl. Magn. Reson.*, 2002, **22**, 484.
44 M. Wilkening and P. Heitjans, *J. Phys.: Condens. Matter*, 2006, **18**, 9849.
45 B. Koch and M. Vogel, *Solid State Nucl. Magn. Reson.*, 2008, **34**, 37.
46 M. Wilkening, W. Küchler and P. Heitjans, *Phys. Rev. Lett.*, 2006, **97**, 065901.
47 M. Wilkening, D. Gebauer and P. Heitjans, *J. Phys.: Condens. Matter*, 2008, **20**, 022201.
48 M. Wilkening, C. Lyness, A. R. Armstrong and P. G. Bruce, *J. Phys. Chem. C*, 2009, **113**, 4741.
49 K. Eichele, *WSolids 1*, Solid-State NMR Spectrum Simulation, Version 1.19.15, University of Tübingen, 2009.
50 M. Wilkening, S. Indris and P. Heitjans, *Phys. Chem. Chem. Phys.*, 2003, **5**, 2225.

51 S. Faske, H. Eckert and M. Vogel, *Phys. Rev. B: Condens. Matter Mater. Phys.*, 2008, **77**, 104301.
52 M. Storek, R. Böhmer, S. W. Martin, D. Larink and H. Eckert, *J. Chem. Phys.*, 2012, **137**, 124507.
53 J. Waugh and I. Fedin, *Sov. Phys. Solid State*, 1963, **4**, 1633.
54 A. Abragam, *The Principles of Nuclear Magnetism*, Clarendon, Oxford, 1961.
55 R. Bertermann and W. Müller-Warmuth, *Z. Naturforsch., A: Phys. Sci.*, 1998, **53**, 863.
56 R. Bertermann, W. Müller-Warmuth, C. Jansen, F. Hiltmann and B. Krebs, *Solid State Ionics*, 1999, **117**, 245.
57 D. Brinkmann, *Prog. Nucl. Magn. Reson. Spectrosc.*, 1992, **24**, 527.
58 A. Kuhn, P. Sreeraj, R. Pöttgen, H.-D. Wiemhöfer, M. Wilkening and P. Heitjans, *J. Am. Chem. Soc.*, 2011, **133**, 11018.
59 P. M. Richards, in *Topics in Current Physics*, ed. M. B. Salamon, Springer, Berlin, 1979, vol. 15.
60 N. Bloembergen, E. M. Purcell and R. V. Pound, *Phys. Rev.*, 1948, **73**, 679.
61 W. Küchler, P. Heitjans, A. Payer and R. Schöllhorn, *Solid State Ionics*, 1994, **70–71**, 434.
62 A. Bunde, W. Dieterich, P. Maass and M. Meyer, in *Diffusion in Condensed Matter – Methods, Materials, Models*, ed. P. Heitjans and J. Kärger, Springer, Berlin, 2nd edn, 2005, ch. 20, pp. 813–856.
63 M. Meyer, P. Maass and A. Bunde, *Phys. Rev. Lett.*, 1993, **71**, 573.
64 K. Funke, *Prog. Solid State Chem.*, 1993, **22**, 111.
65 Similar values (E_a (0.49(1) eV) and $\tau_{c,0}^{-1} = 6(3) \times 10^{12}$ s^{-1}) were obtained by analyzing the rotating-frame SLR NMR data with a Cole–Davidson spectral density function.[76] The distribution parameter α of the Cole–Davidson function turned out to be $\alpha = 0.42(2)$.
66 C. Leon, J. Habasaki and K. L. Ngai, *Z. Phys. Chem.*, 2009, **223**, 1311.
67 M. Vijayakumar, S. Kerisit, Z. Yang, G. L. Graff, J. Liu, J. A. Sears and S. D. Burton, *J. Phys. Chem. C*, 2009, **113**, 20108.
68 M. Wilkening, R. Amade, W. Iwaniak and P. Heitjans, *Phys. Chem. Chem. Phys.*, 2006, **9**, 1239.
69 M. Wilkening, C. Mühle, M. Jansen and P. Heitjans, *J. Phys. Chem. B*, 2007, **111**, 8691.
70 B. Ruprecht, M. Wilkening, R. Uecker and P. Heitjans, *Phys. Chem. Chem. Phys.*, 2012, **14**, 11974.
71 F. Qi, G. Diezemann, H. Böhm, J. Lambert and R. Böhmer, *J. Magn. Reson.*, 2004, **169**, 225.
72 T. Kaib, S. Haddadpour, M. Kapitein, P. Bron, C. Schröder, H. Eckert, B. Roling and S. Dehnen, *Chem. Mater.*, 2013, **24**, 2211.
73 V. Epp, C. Brüning, M. Binnewies, P. Heitjans and M. Wilkening, *Z. Phys. Chem.*, 2012, **226**, 513.
74 F. Qi, C. Rier, R. Böhmer, W. Franke and P. Heitjans, *Phys. Rev. B: Condens. Matter Mater. Phys.*, 2005, **72**, 104301.
75 R. Prasado Rao, N. Sharma, V. K. Peterson and S. Adams, *Solid State Ionics*, 2013, **230**, 72.
76 P. A. Beckmann, *Phys. Rep.*, 1988, **171**, 85.